Enhanced Coherence in Superconducting Circuits via Band Engineering

Luca Chirolli[1,2] and Joel E. Moore[1,3]

[1]*Department of Physics, University of California, Berkeley, California 94720, USA*
[2]*Istituto Nanoscienze—CNR, I-56127 Pisa, Italy*
[3]*Lawrence Berkeley National Laboratory, Materials Sciences Division, Berkeley, California 94720, USA*

In superconducting circuits interrupted by Josephson junctions, the dependence of the energy spectrum on offset charges on different islands is $2e$ periodic through the Aharonov-Casher effect and resembles a crystal band structure that reflects the symmetries of the Josephson potential. We show that higher-harmonic Josephson elements described by a $\cos(2\varphi)$ energy-phase relation provide an increased freedom to tailor the shape of the Josephson potential and design spectra featuring multiplets of flat bands and Dirac points in the charge Brillouin zone. Flat bands provide noise-insensitive energy levels, and consequently, engineering band pairs with flat spectral gaps can help improve the coherence of the system. We discuss a modified version of a flux qubit that achieves, in principle, no decoherence from charge noise and introduce a flux qutrit that shows a spin-1 Dirac spectrum and is simultaneously quite robust to both charge and flux noise.

Introduction.—Superconducting circuits are among the best candidates for quantum computation applications [1–3] and represent an ideal platform for the study and the implementation of artificial quantum matter [4,5]. Among the several varieties, the superconducting flux qubit (FQ) [6] represents one of the early prototypes [7–9] and has recently received renewed interest [10–12]. Its two fundamental current-carrying states correspond to the minima of the circuit Josephson potential, and quantum tunneling (phase slip) generates coherent superpositions. Because of the Aharonov-Casher effect [13,14], the spectrum of the qubit acquires a dependence on gate-controlled offset charges localized on the islands between the junctions [15–20]. The charge degeneracy of the condensate confers a $2e$ periodicity to the spectrum, which resembles a crystal band structure [6,21–23]. In a small loop hosting n-independent superconducting islands, the spectrum in the n-dimensional charge Brillouin zone (BZ) can potentially host Dirac and Weyl points [23] or flat bands, thus simulating quantum materials. An analogous and dual approach has been recently put forward, where the Andreev spectrum of a multiterminal Josephson junction can host Weyl points and can be seen as a kind of topological matter [24,25].

Typically the dependence on the offset charges is minimized, as one of the main sources of decoherence in superconducting qubits is represented by charge noise [6,26–28]. This is the case of the transmon qubit design [29–31], where a large capacitance shunts a small superconducting island, resulting in band flattening as a function of the offset charges, at the price of weakly anharmonic spectra. The same idea has been employed in the later versions of the flux qubit, where a shunt capacitance reduces charge sensitivity [10–12]. On the other hand, drawing from the analogy with crystal band structures, flattening of the bands can result from destructive interference. This is the case in the flat bands of twisted bilayer graphene [32–34], which have recently attracted enormous interest, or the quantum Hall effect, where long-wavelength destructive interference quenches the kinetic energy. A short-wavelength counterpart is represented by lattice models, such as the Lieb or the kagome lattice, where an atomic redundancy at the unit cell level typically produces flat bands. Spectra featuring multiplets of flat bands provide noise-insensitive quantum states, without paying the price of weak anharmonicity.

In this Letter, we employ second-harmonic Josephson junctions (JJs) described by a $\cos(2\varphi)$ energy-phase relation to modulate the Josephson potential at short wavelengths and tailor the details of a structured unit cell. A variety of Josephson energy-phase relations have been discussed in the literature. A relevant example is provided by the 4π Josephson effect in topological superconductors [35], where a $\cos(\varphi/2)$ relation describes single electron tunneling via Majorana zero energy states localized at the junction. Likewise, second-harmonic Josephson energy-phase relations describe tunneling of pairs of Cooper pairs at the junction and several instances have been recently proposed [36,37]. An effective $\cos(2\varphi)$ is realized in parity-protected semiconductor-superconductor qubits [38] through gatemons [39,40], based on semiconducting wires [41,42], or can be obtained by using four nominally equal JJs in a rhombus configuration [43–47]. In turn, the recently introduced bifluxon qubit [48], defined by the

parity of the flux quanta, is based on an effective $\cos(\varphi/2)$ energy-phase relation. These elements, and other instances featuring more general energy-phase relations, provide us with augmented freedom to engineer the Josephson potential and increase the coherence of the system.

The main results of this Letter are a charge-noise-insensitive flux qubit and a robust flux qutrit featuring a spin-1 Dirac spectrum. The former displays multiplets of levels that hardly depend on the offset charges, thus rendering the device basically insensitive to charge noise. The flux qutrit realizes a three-band model mimicking a Lieb lattice, which features a single Dirac cone and an almost flat band in the charge BZ. Despite the increased sensitivity to offset charges, this device shows a good degree of robustness to charge noise and, perhaps more interestingly, an increased insensitivity to flux noise compared to conventional flux qubits.

Charge-noise-insensitive FQ.—The circuit realizing a FQ is composed by a loop interrupted by three JJs and threaded by a flux $\Phi_x = \Phi_0\varphi_x/2\pi$, with $\Phi_0 = h/2e$ the flux quantum [6]. The low-energy states $|L\rangle$ and $|R\rangle$ carry opposite circulating current and correspond to the two minima of the Josephson potential that are degenerate when $\varphi_x = \pi$, as shown in Fig. 1(b). Quantum tunneling generates a matrix element $\Delta = \langle L|H|R\rangle$. A tunneling event accompanied by a 2π phase slip acquires a phase factor that depends on the offset charges via the Aharonov-Casher effect. In an extended picture of the Josephson potential, the low-energy Hamiltonian can be constructed via a tight-binding approach, where the role of the momentum is played by the offset charges $q_1 = Q_1/2e$ and $q_2 = Q_2/2e$.
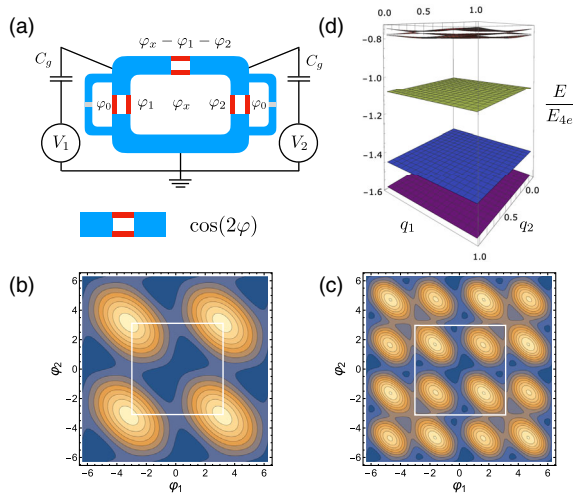

(a)

(b)

(c)

(d)

FIG. 1. (a) Schematics of a charge-noise-insensitive flux qubit employing $\cos(2\varphi)$ JJs, indicated as two parallel red lines. (b) Josephson potential of an ordinary FQ for $\varphi_x = \pi$ and (c) Josephson potential Eq. (2) for the choice $\alpha = 0.8$, $\beta = 0.2$, and $\varphi_x = \pi/2$. In (b) and (c) the unit cell is highlighted in white. (d) Exact spectrum showing the six lowest energy levels as a function of the two offset charges q_1 and q_2.

This way, after recognizing a deformed honeycomb lattice structure, the off-diagonal matrix element is written as $\Delta_{\mathbf{q}} = -\Delta_0 - t_1(e^{2\pi i q_1} + e^{2\pi i q_2})$, in terms of intra- and intercell hoppings Δ_0 and t_1, respectively. The FQ Hamiltonian then reads

$$H = \epsilon(\varphi_x)\sigma_z - \Delta_{\mathbf{q}}\sigma^+ - \Delta_{\mathbf{q}}^*\sigma^-. \quad (1)$$

Here, $\epsilon(\varphi_x) \propto \varphi_x - \pi$ is an energy imbalance between the two current-carrying states occurring when the flux deviates from $\Phi_0/2$, and σ_i are Pauli matrices spanning the $\{|L\rangle, |R\rangle\}$ basis. A two-dimensional Dirac spectrum, gapped by $\epsilon(\varphi_x)$, emerges for $t_1 > \Delta_0$ [6,21–23].

Typically, in order to increase robustness to charge noise, the potential barrier between different cells is increased by reducing the area of one Josephson junction. We now show that we can suppress the tunneling in another way. If we replace all JJs with π-periodic JJs, the Josephson potential simply becomes π periodic. Two branches of $4e$-periodic spectra will appear, one for even and one for odd number of Cooper pairs, shifted by $2e$. If we now shunt the two nominally equal π-periodic JJs with ordinary 2π-periodic JJs with smaller energy, we create a weak modulation of the potential on the scale of the 2π periodicity. As a result of the modulation, the 2π periodicity of the potential is recovered and, accordingly, the $2e$ periodicity of the charge BZ.

The full circuit is schematically depicted in Fig. 1(a). π-periodic JJs are indicated with two red lines. The main loop is composed of three π-periodic JJs, two equal with Josephson energy E_{4e} and the third one with Josephson energy $E'_{4e} = \alpha E_{4e}$. The gauge-invariant phase differences in the main loop can be chosen as φ_1, φ_2, and $\varphi_x - \varphi_1 - \varphi_2$. In addition, the two equal π-periodic JJs are shunted by ordinary 2π-periodic JJs, with Josephson energy $E_{2e} = \beta E_{4e}$, and no flux threads the loop, $\varphi_0 = 0$. For $\beta < 1$, they generate a weak modulation of the Josephson potential, whose full form reads

$$V(\boldsymbol{\varphi}) = -\sum_{i=1,2}[E_{2e}\cos(\varphi_i) + E_{4e}\cos(2\varphi_i)]$$
$$- E'_{4e}\cos[2(\varphi_x - \varphi_1 - \varphi_2)]. \quad (2)$$

Including the charging energy, the full Hamiltonian reads

$$H = 4E_C(-i\nabla_{\boldsymbol{\varphi}} + \mathbf{q})^T\mathcal{C}^{-1}(-i\nabla_{\boldsymbol{\varphi}} + \mathbf{q}) + V(\boldsymbol{\varphi}), \quad (3)$$

with $q_i = C_g V_i/2e$ offset charges controlled by the gate potential V_i via capacitance C_g, $E_C = e^2/2C$, $C = C_J + C_g$, C_J and C'_J are the capacitances of the JJs, and the symmetric capacitance matrix is specified by $\mathcal{C}_{ii} = 1 + c$, $\mathcal{C}_{12} = c$, with $c = C'_J/C$.

The Josephson potential is shown in Fig. 1(c) for the choice $\varphi_x = \pi/2$, $\alpha = 0.8$, and $\beta = 0.2$: it features two global minima at the center of the unit cell and local minima, corresponding to π shifted replica, higher in

energy as an effect of the 2π modulation. The lowest energy current-carrying states are given by the two global minima. Tunneling to the next unit cell necessarily has to take place via virtual processes through local minima. Denoting by Δ_0 and δ_1 the intracell tunneling matrix element between global and local minima, respectively, and t_1 the intercell tunneling matrix elements, with $t_1 < \delta_1 < \Delta_0$, at second-order perturbation theory we have

$$\Delta_{\mathbf{q}} = \Delta_0 + \frac{\delta_1 t_1^2}{\delta E^2 - \delta_1^2}(e^{2\pi i q_1} + e^{2\pi i q_2}), \qquad (4)$$

with δE as the energy difference between global and local minima. Clearly, δE dominates over Δ_0, as the former is on order of E_{2e}, whereas the latter is due to a tunneling process. In the limit $\delta_1, t_1 \ll \Delta_0 \ll \delta E$ the dependence on the offset charges becomes highly suppressed, thus demonstrating the effectiveness of potential engineering. The qubit Hamiltonian is again given by Eq. (1), where now an energy imbalance is set by $\epsilon(\varphi_x) \propto \varphi_x - \pi/2$.

The predictions of the low-energy tight-binding model are checked by diagonalization of the Hamiltonian (3) in the charge basis and the six lowest energy bands are shown in Fig. 1(d). The spectrum has been calculated for $c = 1.9$, $\alpha = 0.8$, $\beta = 0.5$, and $E_C/E_{4e} = 0.055$. On the scale of the full $2e$ charge BZ, the lowest three bands are basically flat. The wave functions of the two lowest energy levels are given by the symmetric and antisymmetric superposition of current-carrying states (not shown).

We now fully address the coherence of the device with respect to charge and flux fluctuations. Following a standard approach [26–28], the dependence of the Hamiltonian on external parameters λ_i is expanded at first order, so that $H_{\text{q-env}} = \sum_i \delta\lambda_i(t)\mathcal{O}_i$, with $\mathcal{O}_i = \partial H/\partial\lambda_i$. This way, charge fluctuations couple to the charge operator $Q_i = (4E_C/e)\mathcal{C}_{ij}^{-1}(-i\partial_j + q_j)$ and flux fluctuations couple to the current operator $I = (2\pi/\Phi_0)\partial V/\partial\varphi_x$. The relaxation time sets the timescale for decay of the excited state $|1\rangle$ to the ground state $|0\rangle$, and by the Fermi golden rule it is given by $T_1^{-1} = \sum_i |\langle 0|\mathcal{O}_i|1\rangle|^2 S_i(\omega_{01})$, with S_i the power spectrum of the fluctuating variable λ_i and $\omega_{01} = E_1 - E_0$ the qubit transition frequency [26–28]. In turn, pure dephasing describes the loss of coherence of superpositions of eigenstates and is therefore sensitive to fluctuations in ω_{01}. Pure dephasing time is estimated as $T_\phi^{-1} = \sum_i |\langle 1|\mathcal{O}_i|1\rangle - \langle 0|\mathcal{O}_i|0\rangle|^2 S_i(0)$ [28,49,50]. Given the form of the relaxation and dephasing rate, two strategies are typically employed to reduce them: either reduce the coupling to the environment, or reduce the fluctuations in the environment. Here we follow the first route and assess the matrix elements of the charge and current operators in the qubit basis.

Pure dephasing can be assessed by directly looking at the dependence of the qubit frequency ω_{01} on charge and flux. In Fig. 2(a) we plot ω_{01} as a function of the normalized
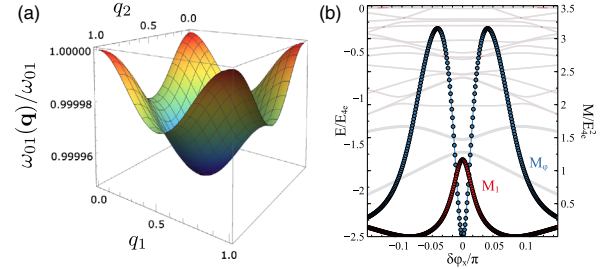

FIG. 2. (a) Energy difference ω_{01} between the two qubit states as a function of the normalized offset charges. (b) Full spectrum highlighting the two lowest energy levels as a function of the applied flux $\delta\varphi_x = \varphi_x - \pi/2$ and matrix elements M_ϕ and M_1 determining the relaxation and pure decoherence rates.

charges on the entire charge BZ. At $q_i = 0, 1/2$ the derivative of ω_{01} is exactly zero and the dephasing time is formally divergent. Such a point is usually termed a sweet spot. More interesting is the bandwidth of energy variation in Fig. 2(a), from which it follows that $4\delta_1 t_1^2/(\Delta_0(\delta E^2 - \delta_1^2)) \simeq 10^{-5}$. This way, $T_1^{-1} \propto 10^{-10}\Delta_0^2 S_q(\Delta_0)$ and $T_\phi^{-1} < 10^{-5}\Delta_0$. We can then conclude that the dephasing time due to charge fluctuations is on order of hundreds of microseconds in the worst cases. This result shows that the coherence of the device can be greatly enhanced through proper design of the Josephson potential. At the same time, flux qubits are very susceptible to flux noise due to the intrinsic dependence of the Josephson potential on the external flux. The latter controls the value of the circulating current and couples directly to one qubit axis in Eq. (1). It immediately follows that the relaxation rate T_1^{-1} has a maximum at $\varphi_x = \pi/2$, for which $\epsilon(\varphi_x) = 0$ and the perturbation is purely off diagonal. Nevertheless, the point $\varphi_x = \pi/2$ represents a sweet spot of formally infinite pure dephasing time T_ϕ and qubit operations can be performed at twice the qubit frequency [51,52]. The exact matrix elements $M_\phi = (\Phi_0/2\pi)^2 |I_{00} - I_{11}|^2$ and $M_1 = (\Phi_0/2\pi)^2 |I_{01}|^2$ determining the dephasing and relaxation rates are shown in Fig. 2(b), together with the circuit spectrum, versus the applied flux. Away from the sweet spot, dephasing due to flux noise can severely affect the device performances. An improvement can be obtained by shunting the third junction with a large capacitance, so to increase the effective mass and reduce the associated tunneling matrix element [10].

Flux qutrit.—We now explain how band engineering can be exploited to design a qutrit system that can retain a high degree of robustness to charge noise, as in the above circuit, while having a reduced sensitivity to flux noise. We consider the system shown in Fig. 3(a). It is similar to that shown in Fig. 1(a), with the difference that the third π-periodic JJ is replaced by an ordinary JJ with Josephson energy E_{2e}', and we set $\varphi_0 = 0$. The Hamiltonian has the form of Eq. (3), with the Josephson potential given by
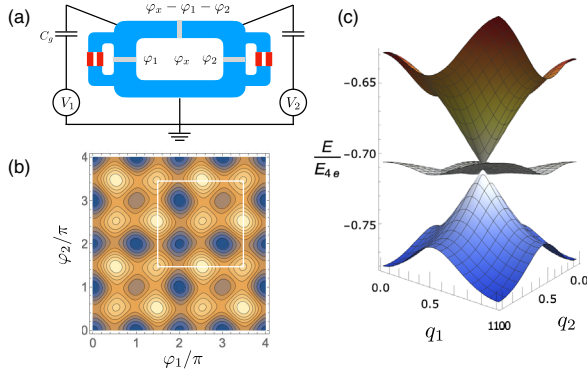
FIG. 3. (a) Schematics of circuit whose spectrum realizes a spin-1 Dirac model. (b) Josephson potential of Eq. (5) for the choice $\beta = 0.3$ and $\gamma = 0.4$, and $\varphi_x = \pi$. The unit cell is highlighted in white. (c) Spectrum of the system showing the first three levels as a function of q_1 and q_2 for $\beta = 0.3, \gamma = 0.352$, and $\varphi_x = \pi$.

$$V(\boldsymbol{\varphi}) = -\sum_{i=1,2} [E_{2e} \cos(\varphi_i) + E_{4e} \cos(2\varphi_i)]$$
$$- E'_{2e} \cos(\varphi_x - \varphi_1 - \varphi_2). \qquad (5)$$

For the choice $\varphi_x = \pi$, the Josephson potential has four minima, a global one at $\boldsymbol{\varphi} = 0$, two local ones at $\boldsymbol{\varphi} = (\pi, 0)$ and $\boldsymbol{\varphi} = (0, \pi)$, and a local one higher in energy at $\boldsymbol{\varphi} = (\pi, \pi)$, as shown in Fig. 3(b). We neglect the high-energy minimum and focus on a low-energy analysis in terms of three minima. Their relative energy can be tuned by varying $\beta = E_{2e}/E_{4e}$ and $\gamma = E'_{2e}/E_{4e}$, and for $\gamma = \beta$ the three minima are degenerate. In order to be good fundamental states, their energy difference must be smaller than the plasma frequency $\omega_P = \sqrt{4E_C E_{4e}}$. This requires the $4e$ Josephson elements to be dominant, with $\beta, \gamma < 1$. Small values of γ ensure that only three fundamental minima determine the low-energy physics. On the other hand, too small values of β call into play the fourth minimum, which would trivialize the analysis.

The three minima define a flux qutrit and form a Lieb lattice in an extended picture of the potential. It is instructive to construct a minimal tight-binding model to describe the low-energy bands. The potential Eq. (5) breaks "mirror" symmetry, $V(-\varphi_1, \varphi_2) \neq V(\varphi_1, \varphi_2)$ and $V(\varphi_1, -\varphi_2) \neq V(\varphi_1, \varphi_2)$, so that two fundamental hoppings t_0 and t_1 can be introduced. A third hopping t_2 has to be introduced in order to account for tunneling through the barrier between two degenerate minima. The effective Hamiltonian reads

$$H_{\mathbf{q}} = \begin{pmatrix} 0 & T(q_1) & \tilde{T}_{\mathbf{q}} \\ T^*(q_1) & -\epsilon(\varphi_x) & T^*(q_2) \\ \tilde{T}^*_{\mathbf{q}} & T(q_2) & 0 \end{pmatrix}, \qquad (6)$$

with $T(q) = -t_0 - t_1 e^{-2\pi i q}$ and $\tilde{T}_{\mathbf{q}} = -t_2(1 + e^{2\pi i(q_1 - q_2)})$. For $t_0 = t_1$ and $\epsilon = t_2 = 0$, the spectrum realizes a well-known spin-1 Dirac Hamiltonian, with three degenerate states at $q_1 = q_2 = 1/2$, a flat band, and a Dirac cone at the center of the charge BZ. Both $\epsilon \neq 0$ and $t_0 \neq t_1$ open a finite gap in the spectrum. For $t_2 = 0$, the model always contains a flat band given by the state

$$u_{\mathbf{q}}^0 = \begin{pmatrix} t_0 + t_1 e^{2\pi i q_2} \\ 0 \\ -t_0 - t_1 e^{2\pi i q_1} \end{pmatrix}. \qquad (7)$$

For $t_2 \neq 0$, the flat band acquires a weak dispersion, and two symmetry-protected Dirac points develop at its crossing with one of the other two bands. The parameters t_0, t_1, and t_2 depend on the potential barriers and the effective capacitances of the circuit. Fine-tuning is possible through flux-dependent Josephson junctions. We numerically diagonalize the Hamiltonian in the charge basis, and the low-energy spectrum is shown in Fig. 3(c) for $\beta = 0.3$, $\gamma = 0.352$, and $E_C/E_{2e} = 0.1$. An approximate spin-1 Dirac spectrum is obtained, with a dispersive Dirac cone and an almost flat band, with deviations due to finite hopping t_2 between degenerate minima.

The flux qutrit so far defined shows interesting coherence properties. Analogously to the case of a qubit, we can define qutrit dephasing and relaxation rates between different levels, $\Gamma_\phi^{nm} = \sum_i |\langle n|\mathcal{O}_i|n\rangle - \langle m|\mathcal{O}_i|m\rangle|^2 S_i(0)$ and $\Gamma_1^{nm} = \sum_i |\langle n|\mathcal{O}_i|m\rangle|^2 S_i(\omega_{nm})$, and associated matrix elements M_1^{nm} and M_ϕ^{nm}, that generically describe the influence of the environment. Clearly the sensitivity to charge noise is enhanced, as shown in Figs. 4(b) and 4(c), due to the simple potential barrier allowing for direct phase slips. Dephasing and relaxation rates all increase toward the center of the charge BZ. However, the point $\mathbf{q} = 0$ represents a sweet spot and M_ϕ^{nm}'s all show a dip at the
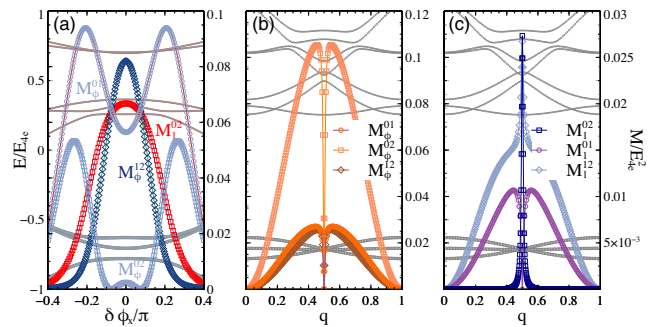

FIG. 4. (a) Matrix elements M_1^{nm} and M_ϕ^{nm} and spectrum of a flux qutrit as a function of the flux bias $\delta\varphi_x = \varphi_x - \pi/2$. (b) Matrix elements M_ϕ^{nm} and spectrum of a flux qutrit as a function of the offset charges $q_1 = -q_2 = q$. (c) Matrix elements M_1^{nm} and spectrum as a function of q. In (a)–(c) thick lines indicate the three lowest energy eigenvalues.

Dirac point, due to level coalescence, whereas only M_1^{01} shows a dip, signaling a transition decoupling. This shows that a certain degree of coherence is still attainable by proper operation. More interesting is the sensitivity to flux noise. In Fig. 4(a) we plot the dependence of the relevant matrix elements, together with the lowest energy levels of the device, as a function of the applied flux φ_x at $\mathbf{q} = 0$. We notice that only the energy of the flatband is sensitive to the applied flux in a good flux window. We then notice that $\Gamma_1^{01} = \Gamma_1^{12} = 0$ within numerical precision. This is due to the fact that the flux in Eq. (6) couples only eigenstates $|0\rangle$ and $|2\rangle$. The physical picture is that the current is zero in all the three lowest energy states at $\delta\varphi_x = 0$. It also follows that, as for the case of the FQ previously described, the associated dephasing rate Γ_ϕ^{02} reaches minimum when Γ_1^{02} is maximum. In turn, Γ_ϕ^{01} and Γ_ϕ^{12} are nonzero in the energy window in which only the flatband energy varies with the flux, and Γ_1^{02} is activated only at the Dirac point. The matrix elements M_1^{nm} and M_ϕ^{nm} also give information on the accessibility of the quantum states by external means for quantum computing purposes. We notice a complementarity between charge and flux dependence and complete access to the qutrit subspace is provided by $M_1^{02}(\varphi_x)$, $M_1^{01}(\mathbf{q})$, and $M_1^{12}(\mathbf{q})$, allowing for coherent manipulations.

Conclusions.—The analysis presented draws an analogy between the $2e$-periodic spectrum of a superconducting circuit and the band structure of a crystal. The inclusion of Josephson junctions characterized by higher-harmonic current-phase relations, of current interest, can be employed to generate modulations of the potential. Relevant tools and ideas can be borrowed from band engineering in crystals and exploited to flatten the dependence of the spectrum on fluctuating external parameters. Our results show that the modification of conventional setups can allow significant gain in robustness to both charge and flux noise, providing a path beyond current limitations of flux qubits.

[1] M. H. Devoret and R. J. Schoelkopf, Science **339**, 1169 (2013).

[2] J. Preskill, Quantum **2**, 79 (2018).

[3] M. Kjaergaard, M. E. Schwartz, J. Braumüller, P. Krantz, J. I.-J. Wang, S. Gustavsson, and W. D. Oliver, Annu. Rev. Condens. Matter Phys. **11**, 369 (2020).

[4] A. Kandala, A. Mezzacapo, K. Temme, M. Takita, M. Brink, J. M. Chow, and J. M. Gambetta, Nature (London) **549**, 242 (2017).

[5] F. Arute *et al.*, Science **369**, 1084 (2020).

[6] T. P. Orlando, J. E. Mooij, L. Tian, C. H. van der Wal, L. S. Levitov, S. Lloyd, and J. J. Mazo, Phys. Rev. B **60**, 15398 (1999).

[7] J. E. Mooij, T. P. Orlando, L. Levitov, L. Tian, C. H. van der Wal, and S. Lloyd, Science **285**, 1036 (1999).

[8] C. H. van der Wal, A. C. J. ter Haar, F. K. Wilhelm, R. N. Schouten, C. J. P. M. Harmans, T. P. Orlando, S. Lloyd, and J. E. Mooij, Science **290**, 773 (2000).

[9] I. Chiorescu, Y. Nakamura, C. J. P. M. Harmans, and J. E. Mooij, Science **299**, 1869 (2003).

[10] J. Q. You, X. Hu, S. Ashhab, and F. Nori, Phys. Rev. B **75**, 140515(R) (2007).

[11] F. Yan, S. Gustavsson, A. Kamal, J. Birenbaum, A. P. Sears, D. Hover, T. J. Gudmundsen, D. Rosenberg, G. Samach, S. Weber, J. L. Yoder, T. P. Orlando, J. Clarke, A. J. Kerman, and W. D. Oliver, Nat. Commun. **7**, 12964 (2016).

[12] L. V. Abdurakhimov, I. Mahboob, H. Toida, K. Kakuyanagi, and S. Saito, Appl. Phys. Lett. **115**, 262601 (2019).

[13] Y. Aharonov and A. Casher, Phys. Rev. Lett. **53**, 319 (1984).

[14] W. J. Elion, J. J. Wachters, L. L. Sohn, and J. E. Mooij, Phys. Rev. Lett. **71**, 2311 (1993).

[15] D. Born, V. I. Shnyrkov, W. Krech, T. Wagner, E. Il'ichev, M. Grajcar, U. Hübner, and H.-G. Meyer, Phys. Rev. B **70**, 180501(R) (2004).

[16] L. Sun, L. DiCarlo, M. D. Reed, G. Catelani, L. S. Bishop, D. I. Schuster, B. R. Johnson, G. A. Yang, L. Frunzio, L. Glazman, M. H. Devoret, and R. J. Schoelkopf, Phys. Rev. Lett. **108**, 230509 (2012).

[17] I. M. Pop, B. Douçot, L. Ioffe, I. Protopopov, F. Lecocq, I. Matei, O. Buisson, and W. Guichard, Phys. Rev. B **85**, 094503 (2012).

[18] M. T. Bell, W. Zhang, L. B. Ioffe, and M. E. Gershenson, Phys. Rev. Lett. **116**, 107002 (2016).

[19] S. E. de Graaf, S. T. Skacel, T. Hönigl-Decrinis, R. Shaikhaidarov, H. Rotzinger, S. Linzen, M. Ziegler, U. Hübner, H. G. Meyer, V. Antonov, E. Il'ichev, A. V. Ustinov, A. Y. Tzalenchuk, and O. V. Astafiev, Nat. Phys. **14**, 590 (2018).

[20] A. Bargerbos, W. Uilhoorn, C.-K. Yang, P. Krogstrup, L. P. Kouwenhoven, G. de Lange, B. van Heck, and A. Kou, Phys. Rev. Lett. **124**, 246802 (2020).

[21] L. Chirolli and G. Burkard, Phys. Rev. B **74**, 174510 (2006).

[22] R. P. Tiwari and D. Stroud, Phys. Rev. B **76**, 220505(R) (2007).

[23] R. Leone, L. P. Lévy, and P. Lafarge, Phys. Rev. Lett. **100**, 117001 (2008).

[24] R.-P. Riwar, M. Houzet, J. S. Meyer, and Y. V. Nazarov, Nat. Commun. **7**, 11167 (2016).

[25] E. V. Repin and Y. V. Nazarov, arXiv:2010.11494.

[26] Y. Makhlin, G. Schön, and A. Shnirman, Rev. Mod. Phys. **73**, 357 (2001).

[27] G. Falci, E. Paladino, and R. Fazio, in *Quantum Phenomena in Mesoscopic Systems*, edited by B. Altshuler, A. Tagliacozzo, and V. Tognetti, International School of Physics E. Fermi. Vol. 151 (IOS Press, Amsterdam, 2003), https://ebooks.iospress.nl/volumearticle/27129.

[28] L. Chirolli and G. Burkard, Adv. Phys. **57**, 225 (2008).

[29] J. Koch, T. M. Yu, J. Gambetta, A. A. Houck, D. I. Schuster, J. Majer, A. Blais, M. H. Devoret, S. M. Girvin, and R. J. Schoelkopf, Phys. Rev. A **76,** 042319 (2007).

[30] J. A. Schreier, A. A. Houck, J. Koch, D. I. Schuster, B. R. Johnson, J. M. Chow, J. M. Gambetta, J. Majer, L. Frunzio, M. H. Devoret, S. M. Girvin, and R. J. Schoelkopf, Phys. Rev. B **77,** 180502(R) (2008).

[31] R. Barends, J. Kelly, A. Megrant, D. Sank, E. Jeffrey, Y. Chen, Y. Yin, B. Chiaro, J. Mutus, C. Neill, P. O'Malley, P. Roushan, J. Wenner, T. C. White, A. N. Cleland, and J. M. Martinis, Phys. Rev. Lett. **111,** 080502 (2013).

[32] R. Bistritzer and A. H. MacDonald, Proc. Natl. Acad. Sci. U.S.A. **108,** 12233 (2011).

[33] Y. Cao, V. Fatemi, A. Demir, S. Fang, S. L. Tomarken, J. Y. Luo, J. D. Sanchez-Yamagishi, K. Watanabe, T. Taniguchi, E. Kaxiras, R. C. Ashoori, and P. Jarillo-Herrero, Nature (London) **556,** 80 (2018).

[34] Y. Cao, V. Fatemi, S. Fang, K. Watanabe, T. Taniguchi, E. Kaxiras, and P. Jarillo-Herrero, Nature (London) **556,** 43 (2018).

[35] A. Y. Kitaev, Phys. Usp. **44,** 131 (2001).

[36] A. Kitaev, arXiv:cond-mat/0609441.

[37] A. Gyenis, P. S. Mundada, A. Di Paolo, T. M. Hazard, X. You, D. I. Schuster, J. Koch, A. Blais, and A. A. Houck, PRX Quantum **2,** 010339 (2021).

[38] T. W. Larsen, M. E. Gershenson, L. Casparis, A. Kringhøj, N. J. Pearson, R. P. G. McNeil, F. Kuemmeth, P. Krogstrup, K. D. Petersson, and C. M. Marcus, Phys. Rev. Lett. **125,** 056801 (2020).

[39] T. W. Larsen, K. D. Petersson, F. Kuemmeth, T. S. Jespersen, P. Krogstrup, J. Nygård, and C. M. Marcus, Phys. Rev. Lett. **115,** 127001 (2015).

[40] F. Luthi, T. Stavenga, O. W. Enzing, A. Bruno, C. Dickel, N. K. Langford, M. A. Rol, T. S. Jespersen, J. Nygård, P. Krogstrup, and L. DiCarlo, Phys. Rev. Lett. **120,** 100502 (2018).

[41] P. Krogstrup, N. L. B. Ziino, W. Chang, S. M. Albrecht, M. H. Madsen, E. Johnson, J. Nygård, C. M. Marcus, and T. S. Jespersen, Nat. Mater. **14,** 400 (2015).

[42] D. J. van Woerkom, A. Proutski, B. van Heck, D. Bouman, J. I. Väyrynen, L. I. Glazman, P. Krogstrup, J. Nygård, L. P. Kouwenhoven, and A. Geresdi, Nat. Phys. **13,** 876 (2017).

[43] G. Blatter, V. B. Geshkenbein, and L. B. Ioffe, Phys. Rev. B **63,** 174511 (2001).

[44] B. Douçot and J. Vidal, Phys. Rev. Lett. **88,** 227005 (2002).

[45] I. V. Protopopov and M. V. Feigel'man, Phys. Rev. B **70,** 184519 (2004).

[46] S. Gladchenko, D. Olaya, E. Dupont-Ferrier, B. Douçot, L. B. Ioffe, and M. E. Gershenson, Nat. Phys. **5,** 48 (2009).

[47] M. T. Bell, J. Paramanandam, L. B. Ioffe, and M. E. Gershenson, Phys. Rev. Lett. **112,** 167001 (2014).

[48] K. Kalashnikov, W. T. Hsieh, W. Zhang, W.-S. Lu, P. Kamenov, A. Di Paolo, A. Blais, M. E. Gershenson, and M. Bell, PRX Quantum **1,** 010307 (2020).

[49] Y. Nakamura, Y. A. Pashkin, T. Yamamoto, and J. S. Tsai, Phys. Rev. Lett. **88,** 047901 (2002).

[50] S. M. Anton, C. Müller, J. S. Birenbaum, S. R. O'Kelley, A. D. Fefferman, D. S. Golubev, G. C. Hilton, H.-M. Cho, K. D. Irwin, F. C. Wellstood, G. Schön, A. Shnirman, and J. Clarke, Phys. Rev. B **85,** 224505 (2012).

[51] N. Didier, E. A. Sete, M. P. da Silva, and C. Rigetti, Phys. Rev. A **97,** 022330 (2018).

[52] S. A. Caldwell *et al.*, Phys. Rev. Applied **10,** 034050 (2018).